In-line monitoring of the fused filament fabrication additive manufacturing process for fibre-reinforced composites

FORSTER, Rosanna, FETEIRA, Antonio <http://orcid.org/0000-0001-8151-7009>, SOULIOTI, Dimitra, GRAMMATIKOS, Sotirios A. and KORDATOS, Evangelos <http://orcid.org/0000-0002-5448-3883>

In-line monitoring of the fused filament fabrication additive manufacturing process for fibre-reinforced composites

Authors: R. Forster*[a] A. Feteira[a] D. Soulioti[a] S. Grammatikos[b] E. Kordatos*[a]

[a]Materials and Engineering Research Institute, Howard Street, Sheffield Hallam University, Sheffield S1 1WB, UK
[b]ASEMlab – Laboratory of Advanced and Sustainable Engineering Materials, Department of Manufacturing and Civil Engineering, Norwegian University of Science and Technology, Gjøvik, 2815, Norway

ABSTRACT

Fused filament fabrication (FFF) is the most widely used additive manufacturing (AM) technique to produce fibre-reinforced polymer matrix composites, due to their low wastage, geometric flexibility and ease of use. However, composites manufactured in this way are highly susceptible to defects such as high void content and poor bond quality at the fibre and matrix interfaces. In the present work, a combination method of Infrared Thermography, Acoustic Emission and micro-computerised tomography was developed for the monitoring of the FFF AM process. Both pure plastic and fibre-reinforced composites were manufactured, and the detection and development of defects created during the printing process were monitored. This combination of techniques allows for detection of defects such as porosity, voids and poor fibre-matrix bonding during printing and the verification of their presence after the printing without the need for destructive testing.

Keywords: In-line monitoring, additive manufacturing, non-destructive evaluation, infrared thermography, acoustic emission, fibre-reinforced composites, polymer matrix composites

*R.Forster@shu.ac.uk, E.Kordatos@shu.ac.uk

1. INTRODUCTION

Fibre reinforced polymer matrix composites (FRPs) are materials which generally have superior properties to conventional materials such as stiffness and specific properties at a reduced weight [1]. Due to these properties, they have a wide variety of uses and applications in sectors ranging aerospace and automotive to biomedical and architecture [2]. Fused filament fabrication (FFF) is the most widely used additive manufacturing (AM) technique to produce FRPs, due to their low wastage, geometric flexibility and ease of use. Traditional modelling and manufacturing of composite materials does not allow for the geometric flexibility facilitated by FFF, due to the need for post-fabrication material removal and its associated wastage and cost [4]. However, composites manufactured in this way are highly susceptible to defects such as high void content and poor bond quality at the fibre and matrix interfaces. These are significant as the strength of the composite as a strong bond is needed between the fibres and the matrix to allow the matrix to transmit an external load to the fibres at the interface [3]. If these defects are not detected, this could lead to severe failure of in-service parts. Detection of such defects has created a new challenge in terms of quality control and assessment.

The application of non-destructive evaluation (NDE) techniques has proven in the past to be challenging [5] however when applied to the FFF process, the techniques can be effective. Infrared Thermography (IRT) [6], Acoustic Emission (AE) [7] and Micro-computerised tomography (Micro-CT) [8] have all found success in effectively determining the presence of defects both pure polymer and fibre-reinforced FFF printed parts. Specifically, IRT and AE are effective when applied together as an in-line monitoring methodology for the process. IRT can be used to determine any uneven material deposition and uneven thermal distribution across the printed layers which can lead to unexpected material cooling behaviours and thermal retention. AE can be used to distinguish between the vibrations and noise of the printing process and an acoustic event from which a defect or anomaly is formed. This in-line methodology can provide a baseline for the assessment of the presence of defects in a sample which can then be backed up using Micro-CT or destructive testing where appropriate.

In this paper, we propose a method of in-line monitoring with the use of IRT and AE benchmarked against Micro-CT to detect the presence of anomalies during the printing process which can lead to the formation of defects in printed parts. This methodology will be applied to both pure polymer fibre-reinforced parts.

2. EXPERIMENTAL SETUP

2.1 In-line monitoring

Printing of the cubed samples was performed on an Anisoprint Desktop Composer A3 printer with a nozzle diameter of 0.4mm. The samples printed were $10mm^3$ cubes with a 5 printed loop brim and 5 printed loop skirt to aid adhesion and material deposition alongside Magigoo PA adhesive glue. The filament of the pure polymer samples was CFC PA with a filament diameter of 1.75mm [9] and the chopped fibre filament was Smooth PA with a filament diameter of 1.75mm [10]. CFC is a non-filled nylon PA12 polymer and Smooth PA is a nylon PA12 filament reinforced with 10% chopped carbon fibre. The smooth PA material profile provided in AURA was used for the chopped fibre printing settings, a custom profile was created for the CFC PA as one was not provided in the software. The printing profiles as well as some of the key parameters are listed in Table 1.

Table 1 - Table showing the printing profiles for the cubed samples.

	0.1mm Macrolayer	0.15mm Macrolayer	0.2mm Macrolayer	0.3mm Macrolayer
Macro Layer Height (mm)	0.1	0.15	0.2	0.3
External Shell Layer Height (mm)	0.05	0.075	0.1	0.15
Plastic Perimeters Layer Height (mm)	0.05	0.075	0.1	0.15
Infill Layer Height (mm)	0.1	0.15	0.2	0.3
Thick support layer height (mm)	0.1	0.15	0.2	0.3
Infill Density (%)	100	100	100	100
First Layer Height (mm)	0.25	0.25	0.25	0.25
Cube Print Time (mins)	57	39	29	19

The experimental setup for the printing process can be seen in Figure 1. The IR results were recorded with a FLIR X6540sc camera with a cooled Indium antimonide (InSb) detector. The capturing frame rate was 101.0Hz with a range of 5-300.0°C, and a field of view (FOV) of 11ºx8.8º. The sensitivity was of >25mK. The camera was connected to a laptop which was recording the output data through FLIR IR software.

The AE data was collected with MISTRAS Micro-II express digital AE equipment, with a 20db gain pre-amplifier (2/4/6) to enhance the AE signals. A wideband AE sensor with a frequency range of 100-900kHz [11] was attached to the print head of the Composer A3 with tape as seen in Figure 1B with ANAGEL ultrasound gel applied to aid in the acoustic coupling. The data was processed in AEWin software.

2.2 Offline Assessment

The equipment used for the offline assessment of the cubed samples was Micro-CT performed on a Bruker Skyscan 1272 equipment. It was used to analyse the internal structure of the printed cubes by loading them onto a raised surface, fixed in place with dental wax and rotated, with images being taken at a set rotation step layer by layer. The filter applied was AL = 0.25mm with an elevation of 12mm. The test selected was a source current of 160µA and a source voltage of 55kV. The pixel resolution was 10µm with averaging frames of 3 and a 0.7° rotation step. The samples were scanned about 180° with a 2016x1344 camera. Once scanning was finished, the images are loaded into NRecon using GPUReconServer where any scanning artifacts such as circle artifacts are removed, and smoothing is performed. The images were then aligned using DataViewer, rendered as a volume render in CTVox and analyses in CTAn where they underwent custom post-processing to allow for porosity percentage measurements.

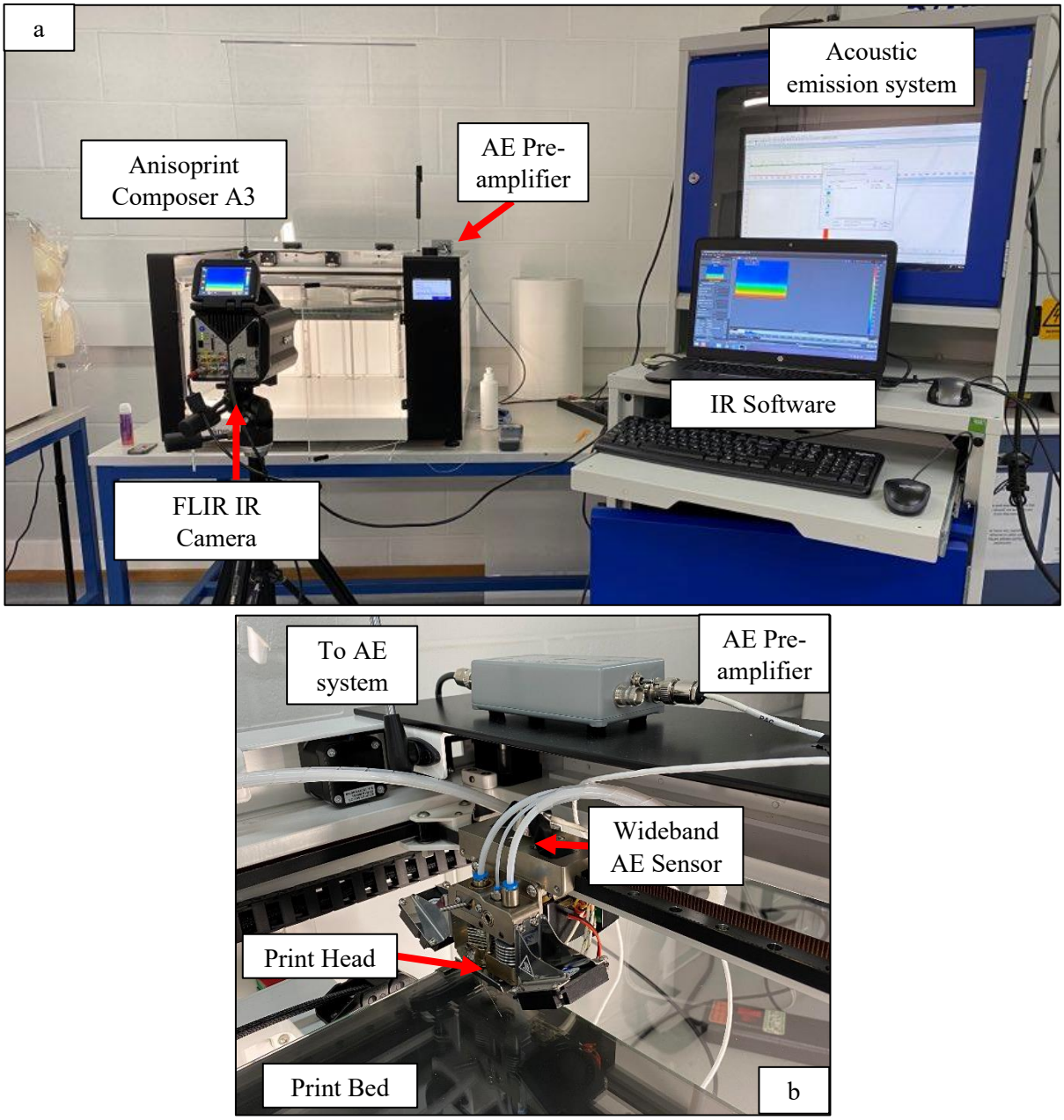

Figure 1 - (a) Experimental setup for the in-line monitoring process with the Composer A3; (b) Setup of the AE sensor attached to the print head with the alignment of the pre-amplifier.

3. RESULTS

3.1 Infrared Thermography

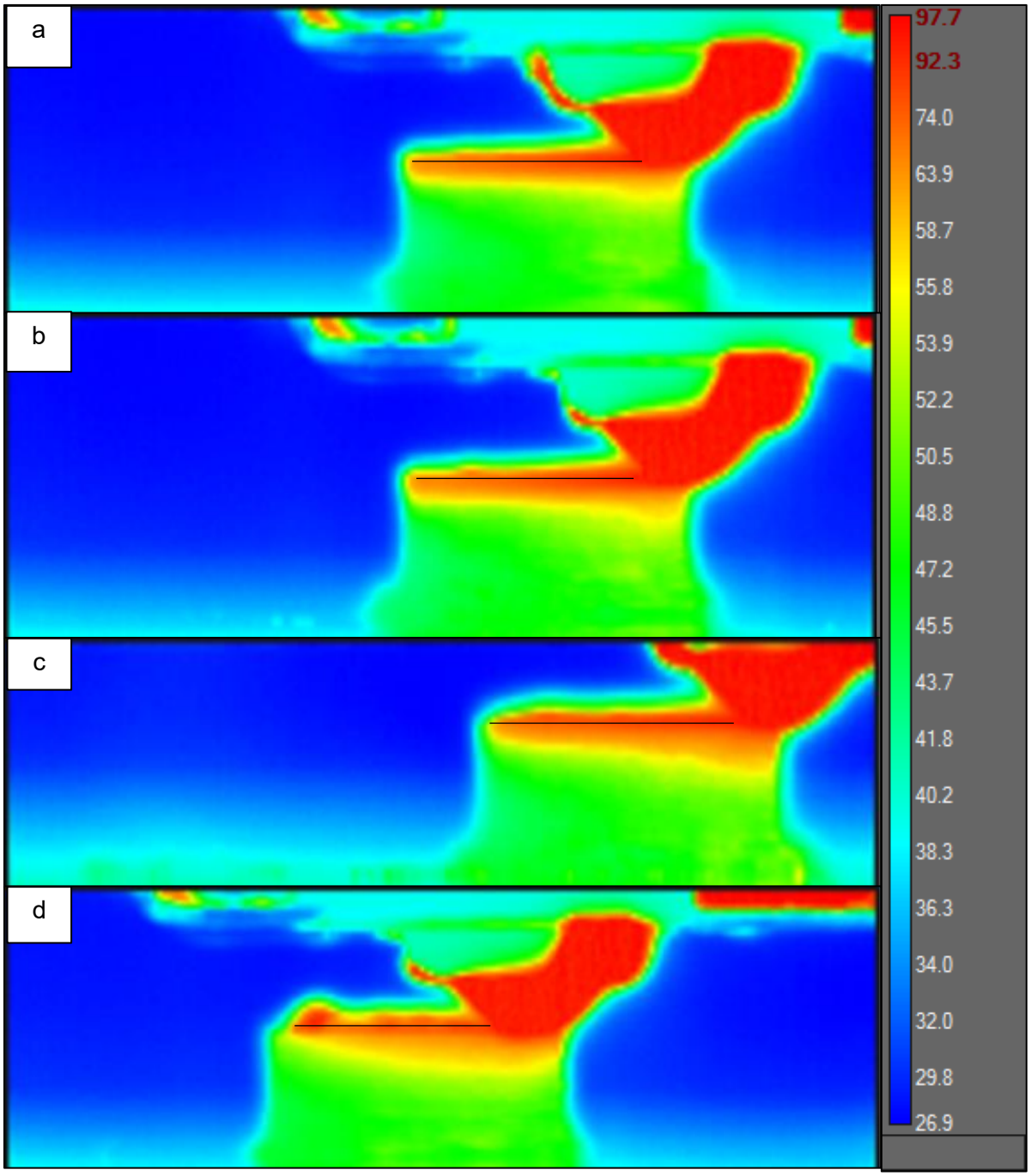

Figure 2 - A- Smooth PA 0.1mm, B – Smooth PA 0.15mm, C - Smooth PA 0.2mm, D – Smooth PA 0.3mm. The black line across the samples represents the line used to draw the profile plot information.

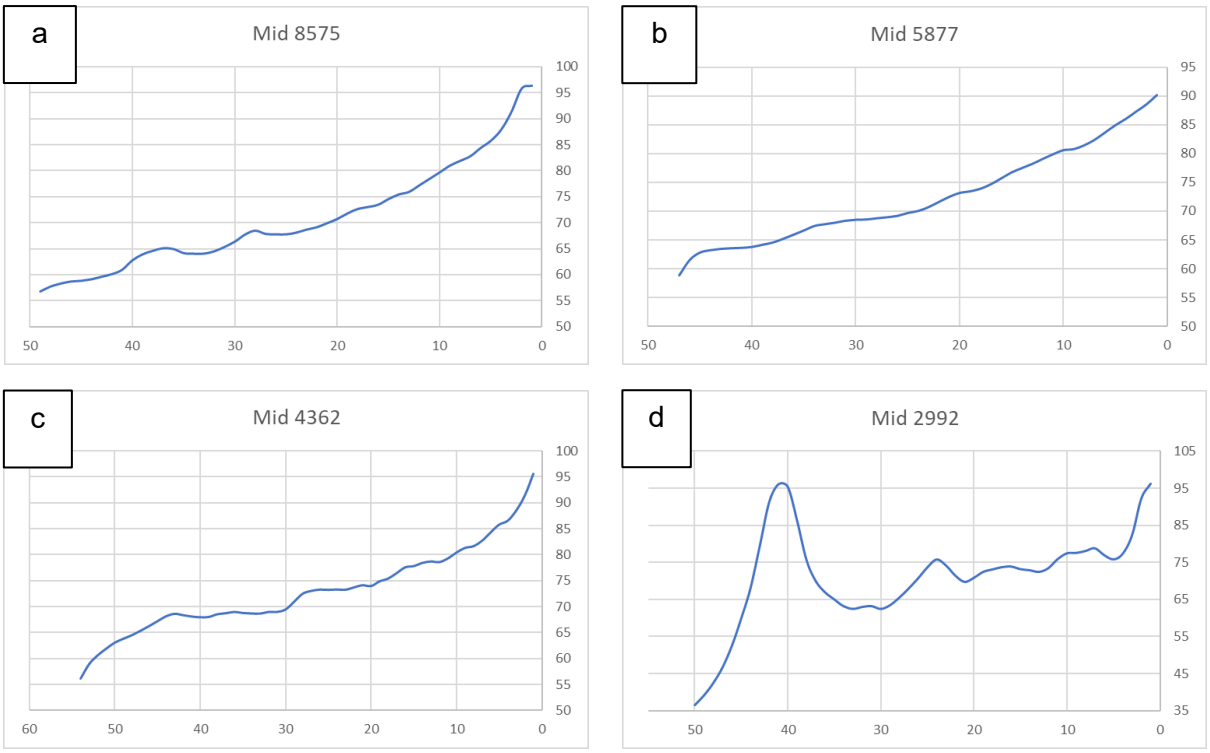

Figure 3 - A- Smooth PA 0.1mm, B – Smooth PA 0.15mm, C - Smooth PA 0.2mm, D – Smooth PA 0.3mm

Figure 2 shows the temperature profiles during the printing process with the results presented graphically in Figure 3. The IRT revealed abnormalities in the thermal distribution of printed material of the 0.3mm macrolayer cube (Figure 3D), with the distribution showing many peaks. This goes against the variation of temperature expected with a steady rise towards the right side of the sample, towards the hotter material and the nozzle. This uneven material deposition seen in Figure 2d and uneven thermal distribution shown in Figure 3d could lead to the formation of defects and porosity as the material cools. Figure 2 also shows a variation in the retained heat in the samples as the print time decreases and the macrolayer size increases, with the 0.1mm macrolayer sample showing less retained heat than the 0.3mm macrolayer sample. This is displayed as the yellow area under the direct print path.

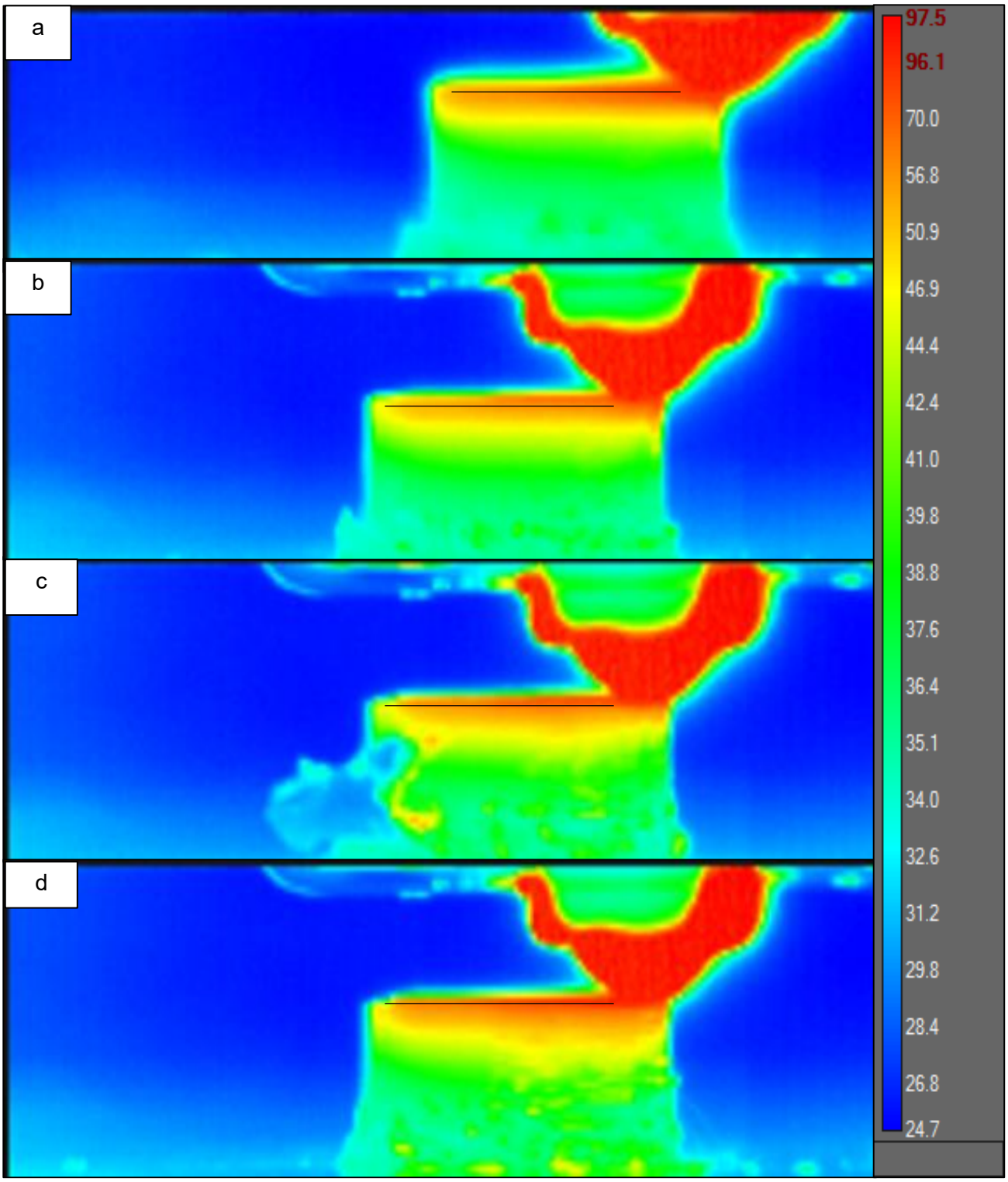

Figure 4 - A- CFC PA 0.1mm, B – CFC PA 0.15mm, C - CFC PA 0.2mm, D –CFC PA 0.3mm. The black line across the samples represents the line used to draw the profile plot information.

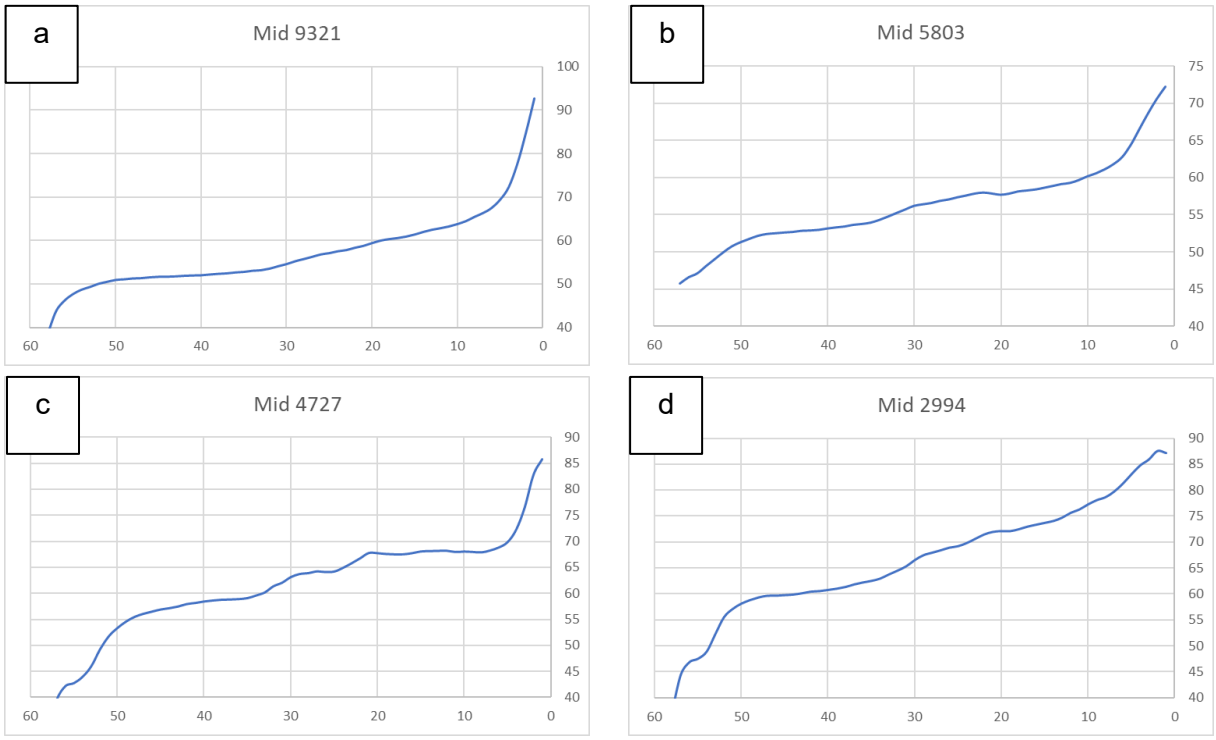

Figure 5 - CFC PA 0.1mm, B – CFC PA 0.15mm, C - CFC PA 0.2mm, D –CFC PA 0.3mm.

Figure 4 shows the temperature profiles during the printing process with the results presented graphically in Figure 5. The IRT showed anomalies in both the 0.2mm (Figure 4C) and 0.3mm macrolayer samples (Figure 4D), with loose material poorly adhering to the print bed and obstructing the view of the camera of the retained heat. However, there is an increase in the retained heat are in the 0.3mm sample compared to the 0.1mm and 0.15mm samples. The CFC PA showed less variation compared to the Smooth PA, with the samples following the expected heat distribution, with hotter material to the right of the images nearing the nozzle, and cooler material to the left.

3.2 Acoustic Emission

Table 2 - Acoustic emission results for printing of the cubed samples showing hits per minute.

Sample Name	Hits/ Min (with 34&36db)
CFC PA 0.1mm	57.719
CFC PA 0.15mm	57.000
CFC PA 0.2mm	63.000
CFC PA 0.3mm	66.579
Smooth PA 0.1mm	59.649
Smooth PA 0.15mm	59.128
Smooth PA 0.2mm	61.517
Smooth PA 0.3mm	62.421

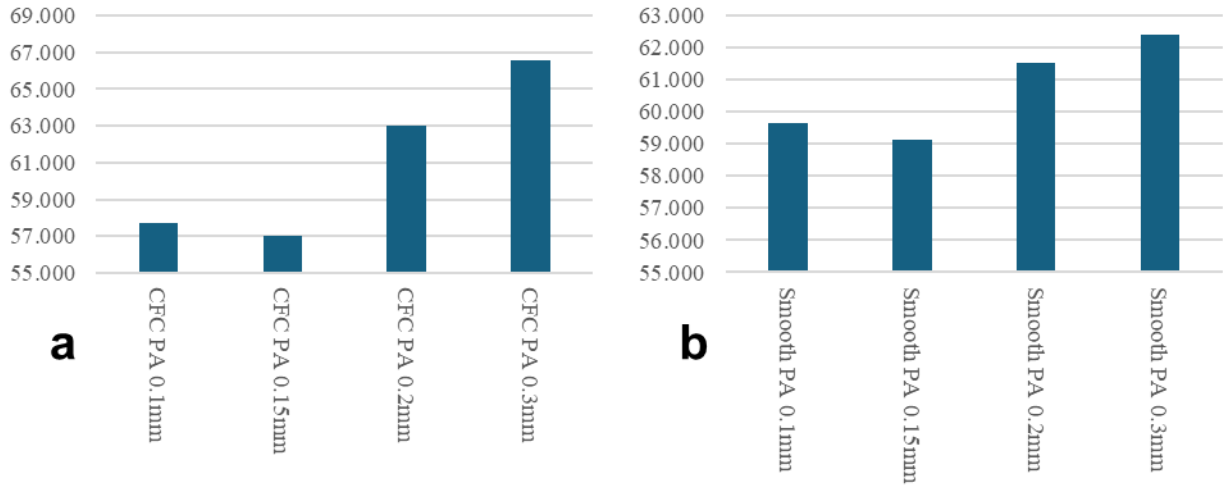

Figure 6 - Acoustic emission results showing hits per minute of a) CFC PA and b) Smooth PA.

The AE results showed multiple events across all the printing profiles and both materials, however when accounting for the printing time, the faster prints with the largest Macrolayer recorded the most hits. Table 2 shows the acoustic emission results for the 8 cubed samples with a trend across both materials showing an increase in hits per minute. This increased by 15.35% between the CFC PA 0.1mm and 0.3mm and a 4.65% increase between the Smooth PA 0.1mm and 0.3mm, displayed graphically in Figure 6. This indicates there are more events which could be indicators of defects with the larger Macrolayer settings compared to the smaller ones. The CFC PA showed a greater variance in results between the different printing profiles with a data set standard deviation of 3.93 compared to the Smooth PA standard deviation of 1.34.

3.3 Micro-CT

Due to the different thresholding required in the custom post-processing of the samples, the CFC PA and Smooth PA infill porosity percentages are not directly comparable however, the trends shown can be discussed.

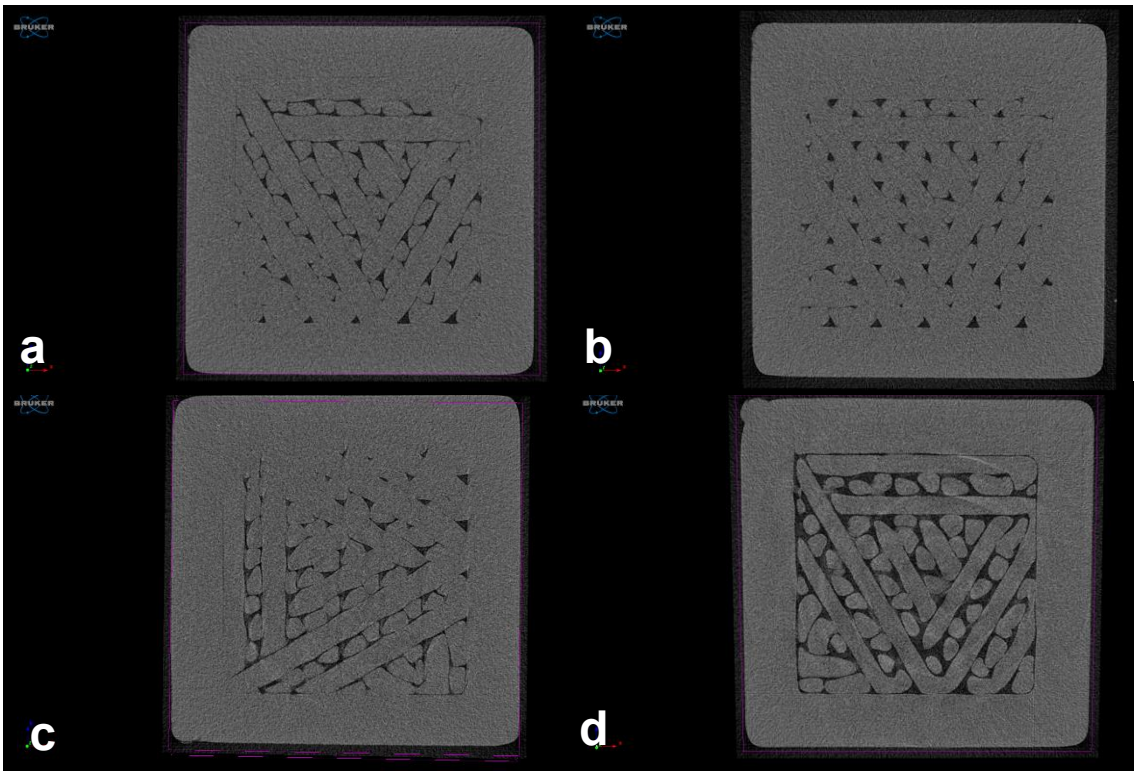

Figure 7 - A- CFC PA 0.1mm, B – CFC PA 0.15mm, C - CFC PA 0.2mm, D – CFC PA 0.3mm

Figure 7 shows the CTVox renderings of the CFC PA samples, with an image slice taken from the infill section of the cubes. There is very similar wall quality between all the samples, with all showing a clear outer section of the cube with no porosity. Porosity appears in the filled section in the centre of the cubes, with the percentage of porosity generally increasing as the macrolayer size increases and the print time decreases. This is further shown in Table 3 where the porosity percentages increase between 0.1mm and 0.2mm. This increase in porosity for the 0.2mm and 0.3mm samples is concurrent with the findings of the in-line monitoring as the IRT showed more retained heat and the AE recorded more events.

Table 3 - Infill porosity percentage for the CFC PA samples. Calculated with a threshold of 55-255.

Sample Name	Infill Porosity Percentage (%)
CFC PA 0.1mm	0.0871
CFC PA 0.15mm	0.0975
CFC PA 0.2mm	0.3057
CFC PA 0.3mm	0.2385

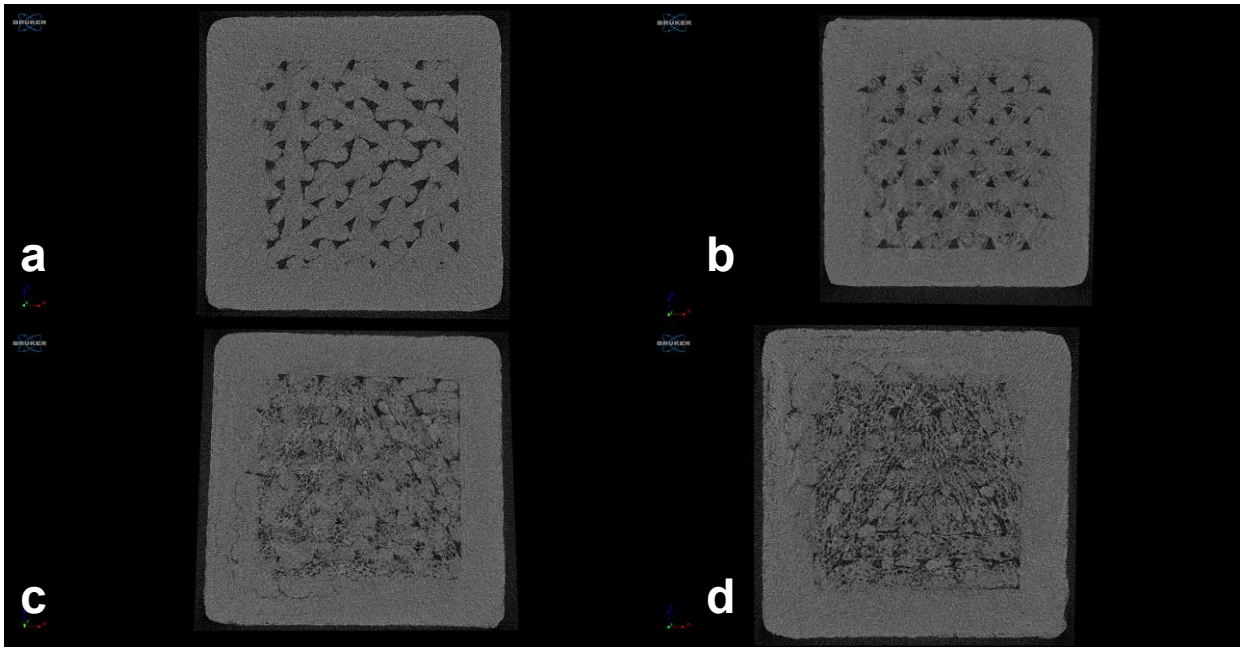

Figure 8 - A- Smooth PA 0.1mm, B – Smooth PA 0.15mm, C - Smooth PA 0.2mm, D – Smooth PA 0.3mm

Figure 8 shows CTVox renderings of the Smooth PA samples, with an image slice taken from the infill section of the cubes. There is a decrease in wall quality as the print time decreases and the macrolayer size increases, with porosity visible in both the 0.2mm and 0.3mm macrolayer cubes. There is also difference in the infill printing itself, with almost no defects been detectable in the 0.1mm printing path. Porosity begins to appear in the "webbed" infill section of the 0.15mm cube, with the 0.2mm and 0.3mm cubes showing more porosity consecutively. This inference is further reinforced with the porosity percentages shown in Table 4

Table 4 - Infill porosity percentage for the Smooth PA samples. Calculated with a threshold of 60-255.

Sample Name	Infill Porosity Percentage (%)
Smooth PA 0.1mm	0.6198
Smooth PA 0.15mm	1.7923
Smooth PA 0.2mm	3.0437
Smooth PA 0.3mm	5.0616

The findings of the offline assessment are concurrent with the indicators displayed by the inline monitoring. In the Smooth PA samples, there is an increase in porosity increasing from the 0.1mm to the 0.3mm Macrolayer samples shown in Table 4. This increase in porosity percentage is concurrent with the increase in AE events across these samples and the IRT.

4. CONCLUSIONS

In this paper, a combination methodology of Infrared Thermography, acoustic emission and micro-computerised tomography was applied to additively manufactured samples produced from pure polymer and short-fibred reinforced composite filament. The methodology was employed to detect defects and anomalies in the printing process, then benchmark the technology against Micro-CT to determine its efficacy.

It was concluded that the in-line monitoring methodology was effective in detecting abnormalities during the printing process such as uneven thermal distribution, uneven material deposition and an increased level of porosity in both pure polymer and fibre-reinforced material. Compared to current methods of detecting these defects, it supplies a non-destructive testing method which can be further benchmarked and backed up by offline assessment. Although requiring further research, this method has proven effective in the detection of abnormalities during the printing process which can lead to the formation of defects.

ACKNOWLEDGEMENTS

For the purpose of open access, the author has applied a Creative Commons Attribution (CC BY) licence to any Author Accepted Manuscript version arising from this submission.

This research was funded by the Sheffield Hallam University Graduate Teaching Assistant Scheme.

REFERENCES

[1] O. Ahmed, X. Wang, M.-V. Tran and M.-Z. Ismadi, "Advancements in fiber-reinforced polymer composite materials damage detection methods: Towards achieving energy-efficient SHM systems," *Composites Part B: Engineering,* vol. 223, p. 109136, 2021.

[2] J. Li, Y. Durandet, X. Huang, G. Sun and D. Ruan, "Additively manufactured fiber-reinforced composites: a review of mechanical behaviour and opportunities," *Journal of Materials Science & Technology,* 2022.

[3] H. Abramovich, "1 - Introduction to composite materials," in *Stability and Vibrations of Thin Walled Composite Structures*, Woodhead Publishing, 2017, pp. 1-47.

[4] C. K. Chua, K. F. Leong and C. S. Lim, Rapid protyping: Principles and Application, 3rd ed., World Scientific, 2010.

[5] T. Smith, J. Failla, J. Lindahl, S. Kim, A. A. Hassen, C. Duty, P. Joshi, C. Stevens and V. Kunc, "STRUCTURAL HEALTH MONITORING OF 3D PRINTED STRUCTURES," in *Solid Freeform Fabrication 2018: Proceedings of the 29th Annual International Solid Freeform Fabrication Symposium – An Additive Manufacturing Conference Reviewed Paper*, 2018.

[6] E. Ferraris, J. Zhang and B. Van Hooreweder, "Thermography based in-process monitoring of Fused Filament Fabrication of polymeric parts," *CIRP Annals - Manufacturing Technology,* pp. 213-216, 2019.

[7] A. Oleff, B. Küster, M. Stonis and L. Overmeyer, "Process monitoring for material extrusion additive manufacturing: a state-of-the-art review," *Progress in Additive Manufacturing,* pp. 705-730, 2021.

[8] J. Soete, B. Badoux, Y. Swolfs, L. Gorbatikh and M. Wevers, "Defect detection in 3D printed carbon fibre composites using X-ray Computed Tomography," in *9th Conference on Industrial Computed Tomography*, Padova, 2019.

[9] Anisoprint, "CFC PA Technical Data Sheet," November 2020.

[10] Anisoprint, "Smooth PA Technical Data Sheet," August 2020.

[11] MISTRAS - Physical Acoustics Corporation, "WD Sensor," 2011. [Online]. Available: https://www.physicalacoustics.com/content/literature/sensors/Model_WD.pdf. [Accessed 17 February 2023].